Using molecular modelling to understand and predict the impact of organic additives as crystal growth modifiers

Franca Jones[a]* and Andrew L. Rohl[b]

[a] *Chemistry, School of Molecular and Life Sciences, Curtin University, GPO Box U1987, Perth WA, 6845 Australia*
[b] *Curtin Institute for Computation and School of Molecular and Life Sciences, Curtin University, GPO Box U1987, Perth WA, 6845 Australia*
** Corresponding author*

Abstract

Empirical molecular modelling was used to investigate the impacts of organic additives on crystal morphology and inhibition. The replacement energy was found to correlate reasonably well with the degree of inhibition as determined from conductivity data. The replacement energy was also able to predict the barium sulfate face on which additive adsorption was most likely. While the ability of the organic functional groups to sit in the vacant sulfate lattice positions (the so-called 'lattice matching' criteria) appears intuitively sensible, it was found that this is not a sufficient criterion to predict real behaviour. A better criterion is the overall replacement energy as it takes into consideration the number of Ba-$O_{organic}$ interactions and whether the adsorption process overall is energetically favourable (by including the hydration energy of the ions). Thus, the replacement energy can successfully predict the effect of organic molecules on the crystal growth modification of barium sulfate.

Keywords: crystallisation, crystal growth modification, molecular modelling

Introduction

Crystallisation is a process often used to separate or purify mixtures. In this context it is a useful process that imparts real and tangible benefits. However, crystallisation is not always wanted or desired, for example in the formation of kidney stones. In industry where hard waters are used, and streams are recycled or waters are mixed, unwanted crystallisation can occur and this process is referred to as scale formation. This can lead to solids precipitating on equipment walls requiring cleaning, shut down of equipment or limiting production, hence the undesirability[1-10]. Barium sulfate crystallisation has been the study of much scientific investigation because it is a simple precipitation system devoid of polymorphism or hydrate formation issues, but it is also a problematic scale product in many industrial processes[4, 6, 10-15]. More generally, wherever there is scale there is an interest in controlling crystallisation in order to mitigate its formation.

Chemical additives can be used to inhibit scale and often these are anionic organic molecules[16-27]. Not surprisingly, it has been found that the deprotonated phosphonate molecule is a more potent inhibitor than its protonated form[28-30]. Also, as the number of phosphonate groups increases so too does the degree of inhibition[31, 32]. It is straightforward to test the effectiveness of these additives in practice, however we are yet to predict their impacts *a priori*. Molecular modelling is a useful tool to understand the interactions between surfaces and additive molecules. It can be used to calculate how organic molecules adsorb (in what configuration) and on which faces adsorption is preferred. Once the

preferred faces where adsorption occurs have been calculated, they can be compared to the experimentally observed particle morphology, thereby testing the efficacy of the model. Molecular modelling of barium sulfate has been previously conducted using empirical potentials by authors such as Allan et al. and Jang et al. amongst others[33-43]. Allen et al.[33] calculated surface energies and the morphology in vacuo, while the latter was a molecular dynamics study that included the hydration of ions. In addition, the work of the de Leeuw group has investigated organic and inorganic impurities on calcite[44-50]. The most relevant literature to this study is the early work of Rohl et al.[36]. This work studied the adsorption of propane-1, 3-diphosphonate on barium sulfate and reported that the most energetically favourable faces for adsorption were the (100), (011), and (010) barite surfaces. Experimental results showed that the presence of the diphosphonate molecule caused the expression of the barite (011) face at low concentrations while the [001] zone appeared to be attacked at high concentrations, in general agreement with the modelling.

Ideally, modelling is best utilised when both simulation results and experimental data can inform each other. Previous research has presented the hypothesis of 'lattice matching' (or molecular recognition) to predict the effectiveness of the organic anion to inhibit[51-56], but even the early study by Rohl et al.[36] suggested that this hypothesis was too simplistic. Over the past decade, we have extended this work to examine various parameters.

Lattice matching

Lattice matching refers to the ability of the inhibitory molecule to adsorb onto (or at least interact with) one or more faces of the solid such that the functional groups 'match' (though this doesn't need to be exact) the position of a cation or anion (depending on the charge of the functional group) in the lattice[51-56]. Intuitively, this makes sense. For example, in barium sulfate if an inhibitor could replace the sulfate in the sulfate lattice position, it should maximize its interactions with the barium ions. However, lattice matching has been used as a criterion for both inhibition and promotion. Thus, more understanding is required into what criteria are suitable and how inhibition can be predicted.

To this end we have modelled adsorption of various organic molecules on the terraced (flat surfaces) faces of barium sulfate (or barite, the mineral name) and compared our computational results to the results of our experiments. Most importantly, it was the aim of this body of work to determine whether modelling could predict the ability of the organic additives to inhibit precipitation. In addition, lattice matching was compared to the replacement energy calculation (i.e. the energy to replace sulfates in the surface with the adsorbed organic) to see which method best predicts inhibition impacts.

Materials and Methods

Various experimental methods were used to measure the processes (nucleation, growth) during crystallisation and the reader is directed to the references[29, 31, 32, 35, 38, 40, 57-68] for detailed information.

Correlating computational data with experimental results

Morphology

Static crystallisation experiments were undertaken whereby a fixed concentration of barium ions, organic acid and water were equilibrated to ~pH 6 and then equimolar sulfate ions were added to commence crystallisation. After three days glass cover slips, which were

used to make collection easier, were removed, washed and assessed with scanning electron microscopy (SEM). The morphology of barium sulfate in the absence of inhibitors is shown in Figure 2d. If the organic adsorbs significantly to a face, it is assumed to slow down the growth rate of that face. Thus, if that face is already observed in the control morphology, the presence of the impurity should increase the relative importance of that face while if it is absent in the control morphology, it would be expected to express that face in the presence of the impurity.

Thus, the approach to gaining an understanding of the impact of each additive on morphology was to determine the lowest three replacement energies from the computational work and see whether the expected changes were observed in the morphology of the crystals.

Degree of inhibition by comparison to conductivity data

Conductivity measures the mobility of ions in solution. As barium sulfate crystallisation involves barium ions coming together with sulfate ions to produce a non-charged solid, conductivity decreases as crystallisation proceeds. The linear section of the conductivity versus time curve is normalised to the control (values of which can be seen in Table 6) before being plotted to give a relationship between the de-supersaturation rate and the concentration of impurity. Generally, the lower the concentration of impurity required to inhibit the de-supersaturation rate, the stronger the impurity is as an inhibitor. However, some organics have a complex relationship between the degree of inhibition and their concentration. In these cases, the graph can be more useful.

The average replacement energy is then compared to the 'strength' of inhibition based on the concentration required to inhibit crystallisation.

Molecular modelling

Empirically derived potentials are used throughout and the potential values can be found in the cited literature.

Barium Sulfate. Initially, the model must be validated by comparison to known values of the crystal properties to confirm that the model is suitable. In this work, we started with the empirical potentials for barium sulfate from Allan et al. (model 2)[33] and subsequently fitted to the experimentally known crystal structures of both strontium and barium sulfate using GULP[69, 70] (Table 1 below).

Table 1. Calculated and experimental lattice parameters (Å) for both strontium and barium sulfate using the empirical potentials described in Ref 71

	barium sulfate		strontium sulfate	
	Calculated	Experimental[72]	Calculated	Experimental[73]
a	8.95	8.88	8.39	8.36
b	5.45	5.46	5.38	5.35
c	7.15	7.16	6.84	6.86
Vol	346.1	346.9	308.6	306.8

The calculated morphology of barium sulfate was then calculated by two methods. The first method was via the surface energy, which looks at the energy difference between surface ions and the bulk normalised for surface area according to (eq 1).

$$E_{surf} = (E_{reg1} - nE_{bulk})/A \quad -(1)$$

here E_{reg1} is the energy of region I, E_{bulk} the bulk energy of the unit cell, n the number of unit cells in region I, and A is the simulation cell area. This can be calculated because the simulation slab is split into two regions. Atoms/ions in region I are able to move during the energy minimisation and this represents the surface. Atoms/ion in region II are fixed (see Figure 1) and so this region represents the bulk interaction on the surface in region I. The whole system is periodic in 2 dimensions (directions relating to a and b).

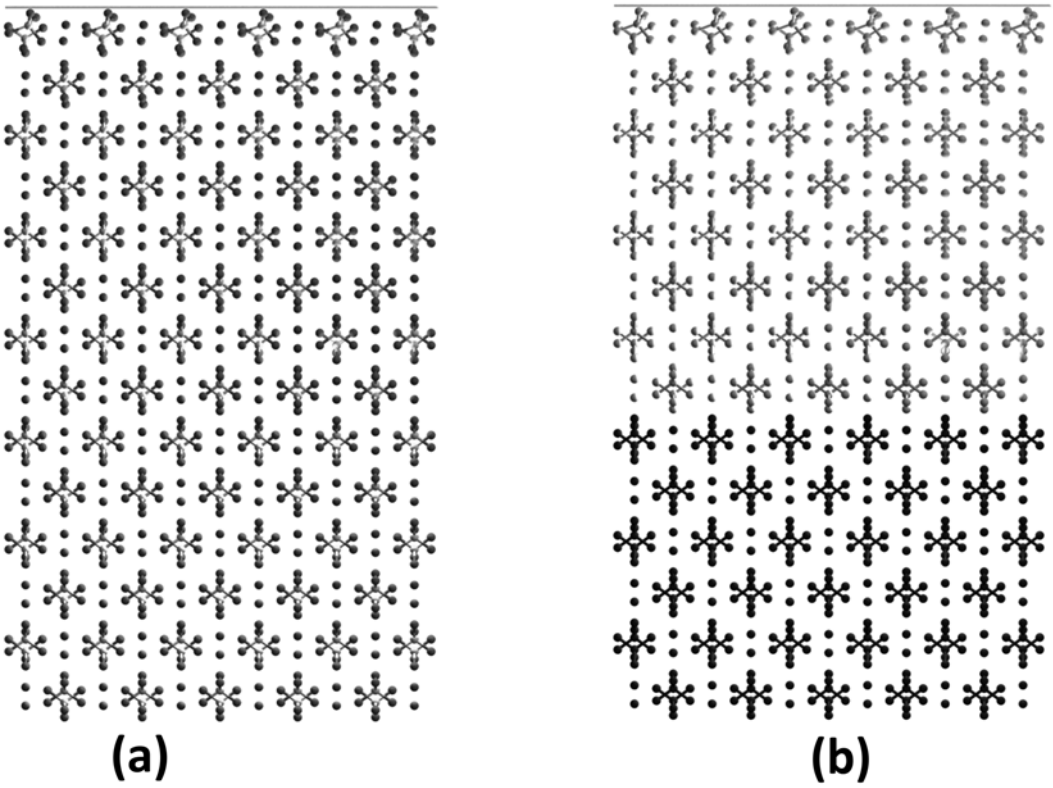

Figure 1. Simulation cell used in the modelling work; (a) the atoms are shown in ball and stick representation while in (b) the two regions are highlighted (light grey = surface – allowed to relax, dark grey = bulk – fixed positions); both are viewed from the <100> direction (adapted from Ref 70 with permission from American Chemical Society)

Crystal faces with lower surface energies tend to be slower growing and thus are more dominant morphological faces. The morphology determined using the surface energy calculation is called the "equilibrium" morphology. The other way of calculating morphology is to use the attachment energy method. Here, the energy of attaching another 'slice' of the crystal (of depth d_{hkl}) to the surface is found. The smaller the attachment energy for a face, the more likely the face will be dominant in the morphology of the particle. This is known as the "growth" morphology. Each face can be terminated at different surfaces and so all must be assessed to find the termination with the lowest energies. The faces to be modelled were based on looking at the 15 faces with the smallest interplanar spacings. For each, those with the lowest energy terminations were chosen. The surfaces were allowed to minimise (i.e. relax), and on completion a morphology was generated using these relaxed energies *via* the Wulff plot in GDIS[74] (see Figure 2a &b). Comparison to experimental results shows that the equilibrium form reasonably reproduces the particle morphology at low supersaturation (S) values while the attachment energy calculations better reproduces the curvature seen at higher supersaturations.

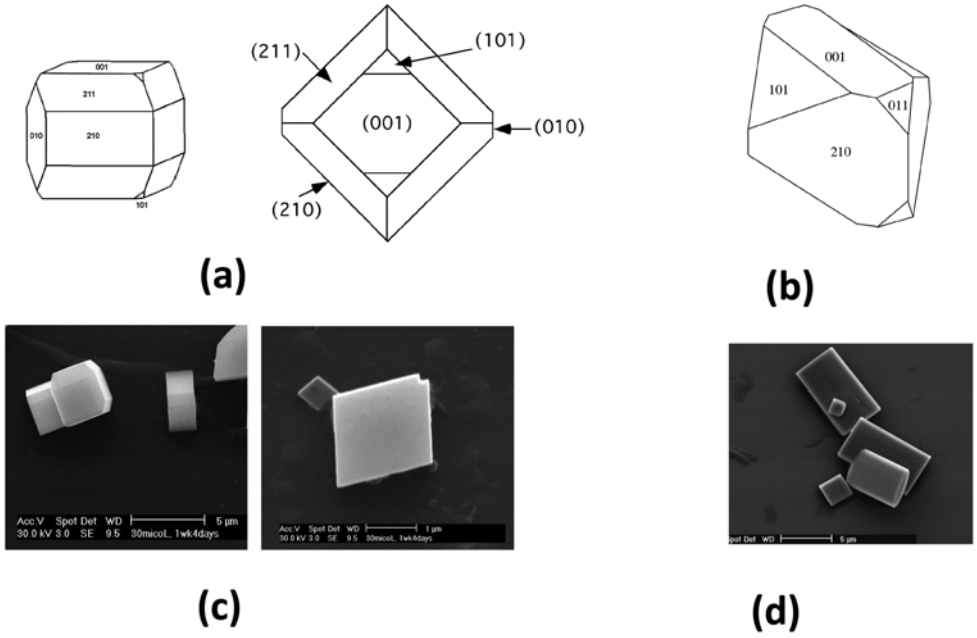

Figure 2. Barium sulfate morphology determined by (a) the surface energy or (b) the attachment energy (c) SEM of particles formed at S=5 (adapted from 71 with permission from American Chemical Society) (d) SEM of particles formed at S=25

While the faces are easily indexed at low supersaturations, at higher supersaturations as shown in Figure 2d, the end faces are (001) with curved (hk0) faces.

A barium sulfate cell large enough to fit the organic growth modifier without interactions with the same molecule in the next cell (due to the 2D periodicity) was then constructed. For the organic molecules, the empirical potentials used can be found in the various references[59, 62, 65, 71, 75]. GDIS[74] was used to construct the simulation cells and GULP[69, 70] was the energy minimizer engine used. To maintain charge neutrality of the system as a whole, equivalent sulfate groups were removed from the surface as the charge on the molecule. Similarly, in order to have some confidence that the minimised energy was the global minimum many different initial configurations were trialled. The potentials used are both intra- and inter- molecular in nature so that all interactions are accounted for. Naturally, the energy of the whole system (crystal and the organic) was minimised to find the final structure. For a more detailed account the reader is directed to references[59, 62, 65, 71, 75]. The replacement energy (to replace sulfates in the surface with the organic) was then calculated for each crystal surface and additive according to:-

$$(BaSO_4)_x\ (s) + Organic^{n-}\ (aq) \rightarrow (BaSO_4)_{x-n/2}Org\ (s) + n/2\ SO_4^{2-}(aq) \quad -(2)$$

$$E_{repl} = (E_{final} + n/2[E_{hyd,\ sulf} + E_{sulf}]) - (E_{init} + E_{hyd,\ org} + E_{org}) \quad -(3)$$

Where E_{repl} is the replacement energy, E_{final}, E_{init} is the final (with adsorbed organic) and initial energy respectively, E_{org} etc. is the energy for the isolated ion in the gas phase and E_{hyd} is the hydration energy for the ions. The more negative the replacement energy, the more likely is the replacement reaction. This energy is assumed to be representative of how strongly the organic adsorbs onto the crystal surface.

Results

Many organic additives have been investigated for inhibitory action or crystal growth modification. However, an impact on growth does not necessarily translate to an impact on

morphology. The greatest impact on morphology will be when the organic additive adsorbs preferentially on only a select few faces. In comparison, when the organic adsorbs onto all faces equally, less impact on the morphology is observed but the organic might still impact on the nucleation and/or growth rate. Thus, different experimental data is needed to gauge the overall and specific impacts of the organic additive on the crystallisation processes. We use the relative values of the replacement energies to gain an insight into which faces are predicted to be most impacted and which additives are predicted to be more potent. These predictions are then compared to the appropriate experimental results[29-32, 57, 59-61, 63-66, 76, 77] to determine the ability of our model to predict such behaviour. When the model is successful in predicting behaviour, we can then further use the modelling to gain insight into the mechanisms of action.

Propane-1, 3-diphosphonate

Initially, in order to validate our potentials and the methodology, we compared our results for propane-1,3-diphosphonate molecule[36] with the previous work in the literature[71]. The replacement energies (Table 2) were found to be more negative: ~ -(1100-700) kJ mol^{-1} versus ~ -(300-100) kJ mol^{-1} due to the different forms of potentials used. The replacement energies for the different faces had, however, very similar order despite these differences. In fact, the three most energetically favoured faces were the same.

Number of phosphonate groups[71]

Systematically changing the number of phosphonate groups on a molecule was achieved by maintaining the backbone of the organic but altering the number of functional groups (MNDP – two, NTMP – three, EDTP – four). The modelling results can be found in Table 2. Generally, increasing the number of phosphonate moeities decreases the replacement energy. This suggests that EDTP should be the strongest inhibitor. As comparison to Table 5 and 6 shows, this is indeed the case.

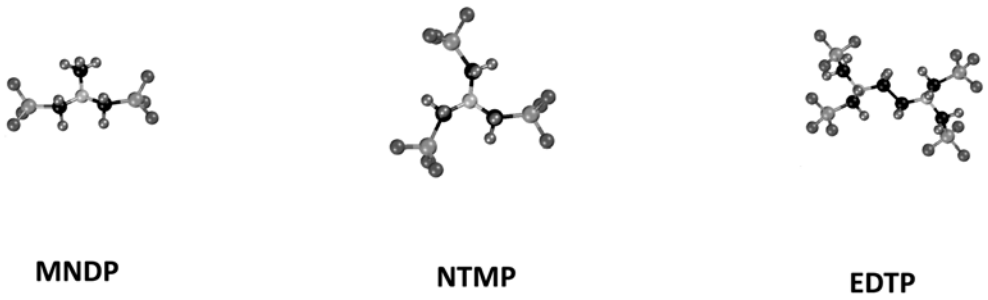

Figure 3. Organic molecules modelled in Ref 71 (with permission from American Chemical Society). MNDP = methylenenitrilodiphosphonic acid, NTMP = nitrilotrismethylenephosphonic acid, EDTP = ethylenediaminetetraphosphonic acid

The modelling results on MNDP[70] and the replacement energy (Table 2) show that the phosphonate functional groups sit in the vacant sulfate positions as much as possible. On the (011) face at least one phosphonate group cannot fit exactly in the vacant sulfate position, showing the impact of steric factors on 'lattice matching'. Comparing the MNDP

and the propane-1,3-diphosphonate molecules (discussed previously) shows that the lowest three replacement energies are the same for these two molecules suggesting that their impacts on morphology should be similar. Beyond the lowest three replacement energies, there are differences and these are probably due to the differences between the two molecules, MNDP has a methyl group and a nitrogen atom. In addition, MNDP has a more negative solvation energy. This would lead to a less surface-active molecule than the propane diphosphonate molecule, leading to more positive replacement energies for MNDP.

For NTMP, regardless of face, the backbone is slightly above the surface. This suggests a lack of favourable interactions between the CH_2 backbone and the surface. From conductivity studies[29, 65, 66], we have observed disc like particles formed at 0.037 mM of NTMP. These disk-shaped particles were examined by TEM and were single crystals (Figure 4a), according to selected area electron diffraction (SAED) patterns. The replacement energy calculations (Table 2) show that the most favoured faces for NTMP to adsorb are calculated to be the (100a), (011) and the (101). By indexing the SAED patterns the "flat" face of the disk was found to be the (100) plane. The (100a) face was also the lowest replacement energy calculated for NTMP from the simulations and shows how the model can be used to predict the impact on morphology in the presence of organic molecules.

For EDTP, the barite structure is almost unchanged by the presence of the organic molecule. Also, similar configurations of the EDTP molecule are observed in the minimised model for the (100a) and (001) surfaces despite these faces being quite different. The EDTP backbone is again found above the surface, regardless of face. The most favourable faces for EDTP to replace the sulfates (Table 2) are the (100) faces and the (001) and (210) faces. Thus, the model would predict that these faces should be stabilised compared to the control particles (which are similar to those in Figure 2d). Figure 4b shows the particles formed at low concentrations of EDTP. The particle surfaces have been assigned, the basal face is the (001) face while the side faces are the (210) and (100) faces. Thus, once again the modelling correlates with the resultant morphology.

In terms of the predicted inhibition based on replacement energy calculations, the average replacement energy follows:

EDTP< NTMP< di-phos molecule < MNDP

While experimental data for the impact of the propane-1,3-di-phosphonate molecule on the de-supersaturation rate of barium sulfate is not available, the other molecules do indeed follow this expected trend (see conductivity results in Table 6) whereby the EDTP is the most potent inhibitor (requires the least concentration to inhibit) followed by the NTMP and MNDP molecules.

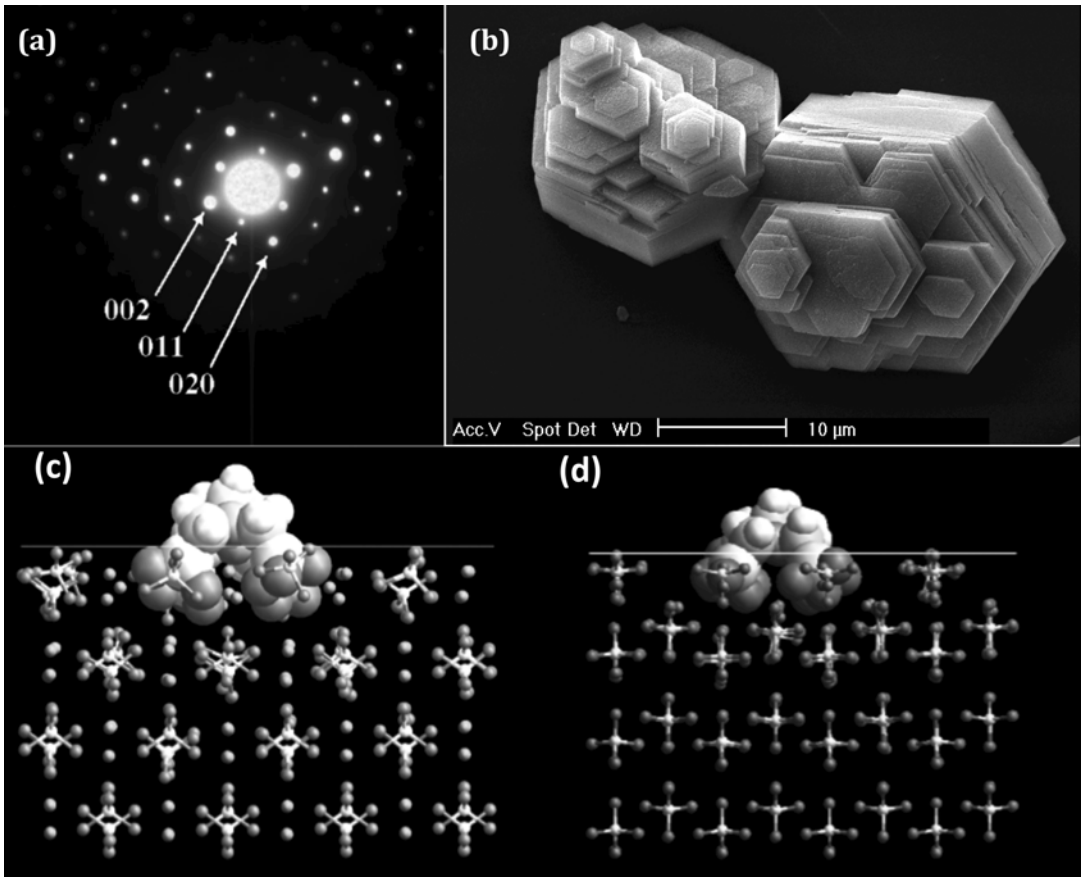

Figure 4. (a) SAED obtained from barite particles crystallised in the presence of 0.037 mM NTMP[71] (with permission from American Chemical Society) and (b) barium sulfate particles crystallised in the presence of 0.01 mM EDTP aged for 12 months. Minimised structure of EDTP on barium sulfate for the (c) 001 and (d) 100a face.

It was suspected that despite the imperfect 'lattice matching' by these organic additives, that an important parameter is the number of Ba^{2+} to $O_{organic}$ interactions. It is found that there are 22 barium to additive-oxygen atomic distances less than 3 Å for EDTP on the (100a) face. This distance can vary from 2.2 to 2.9 Å, with the average being 2.3 Å. Differences in the replacement energy are also observed even when normalised by the number of phosphonate groups (Table 3), supporting that more than just the number of phosphonate groups is acting on the replacement energy.

Table 2. Replacement energies (kJ mol^{-1}) for the phosphonate containing molecules for the different faces modelled

Face	Propane-1,3-diphosphonate	MNDP	NTMP	EDTP
(001)	-806.37	-610.53	-1011.80	-2077.04
(210)	-780.99	-533.25	-991.95	-2077.08
(211)	-809.57	-615.00	-1184.57	-1781.81
(010)	-878.80	-686.44	-1149.29	-1989.40
(011)	-985.89	-818.14	-1364.84	-1906.02
(101)	-751.16	-674.02	-1256.13	-2071.72
(100a)	-1066.96	-921.11	-1486.92	-2405.19
(100b)	-767.04	-460.16	-1037.54	-2196.25
Average	-855.85	-664.83	-1185.38	-2063.07

Table 3. Replacement energies (kJ mol^{-1}) for the phosphonate containing molecules for the different faces modelled normalised by the number of phosphonate groups.

Face	Propane-1,3-diphosphonate	MNDP	NTMP	EDTP
(001)	-403.2	-305.3	-337.3	-519.3
(210)	-390.5	-266.6	-330.7	-519.3
(211)	-404.8	-307.5	-394.9	-445.5
(010)	-439.4	-343.2	-383.1	-497.4
(011)	-492.9	-409.1	-455.0	-476.5
(101)	-375.6	-337.0	-418.7	-517.9
(100a)	-533.5	-460.6	-495.6	-601.3
(100b)	-383.5	-230.1	-345.9	-549.1

There were aspects that were predicted from modelling but were not observed experimentally. These were the impact on the (100a) face predicted in the presence of the MNDP and the conductivity results that showed no inhibition occurred in the presence of the MNDP molecule. However, as noted later, this is best explained by the speciation of the organic molecule (degree of de-protonation) in the experiment compared to the model.

Carboxylate versus phosphonate[62, 75]

The average replacement energy for adsorption of the carboxylate, ethylenediaminetetraacetic acid (EDTA), onto barium sulfate was found to be -598.66 kJ/mol. This significant difference in replacement energy is essentially due to the charge difference between the carboxylate (-1) and the phosphonate (-2) group. Both molecules can lattice match on some faces of barium sulfate and so, this alone cannot be used to understand the inhibitory action. The criterion introduced above of the number of $Ba\text{-}O_{organic}$ interactions less than 3 Å can be applied here too. For EDTA, on the most energetically favoured face, there are 13 interactions while EDTP has 22 on the most energetically favoured face. The two most negative replacement energies for EDTA to adsorb onto barite are the (011) and the (100a) (see Figure 5c) and this impact is seen morphologically. The particles change in morphology such that rounded tips are seen (these indicate expression of the (011) faces) and there are flat sections on the barium sulfate

particles (which were found at higher concentrations to be (100) from TEM analysis[62, 75], see Figure 5a).

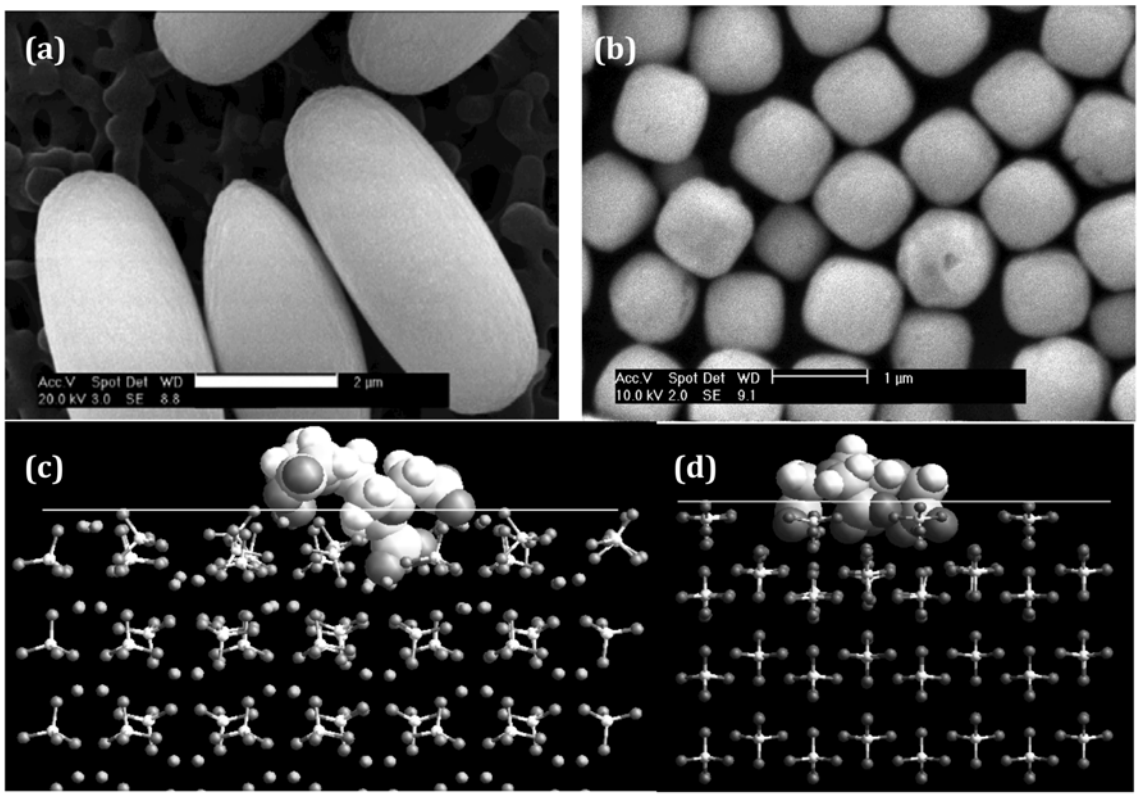

Figure 5. SEM image of barium sulfate crystallised with (a) EDTA at 0.049 mM (Reproduced from Ref 75 with permission from Elsevier) and (b) NTA at 0.078 mM (Reproduced from Ref. 31 with permission from The Royal Society of Chemistry) present. The minimised energy configurations of EDTA on barium sulfate for the (c) 011 and (d) 100a face.

Hydrogen bonding[31, 65]

The possibility of a molecule to hydrogen bond was investigated by modelling nitrilotriacetic acid (NTA) and the zwitterion of NTA[31, 65]. In this way, by looking at essentially the same structure, the impact of hydrogen bonding rather than functional group can be probed. The degree of hydrogen bonding was determined by analysis of the interatomic distances. The results from this work showed that indeed the presence of hydrogen bonding did impact the final replacement energy calculated. The difference in replacement energy was up to ~30% on some faces (see Table 4). On all faces, however, the additional hydrogen bonding made adsorption more thermodynamically favourable.

Note that the average replacement energy predicts the hydrogen bonded NTA to inhibit similarly or slightly better than the EDTA molecule despite the higher number of carboxylate groups in the latter. The NTA molecule was found to impact the morphology (Figure 5b) and the growth rate of barium sulphate experimentally. The results from conductivity in Table 6 show that NTA is similar in inhibition to EDTA as would be expected given their similar average replacement energies.

Table 4. Replacement energies (kJ mol^{-1}) for NTA and the zwitterion containing NTA on different barium sulfate faces

Face	NTA	NTA-zwitterion	% difference
(001)	-437.9	-496.1	12
(210)	-332.6	-404.0	18
(211)	-446.4	-612.1	27
(010)	-852.1	-948.2	10
(011)	-522.7	-575.1	9
(101)	-541.3	-560.3	3
(100a)	-590.4	-685.7	14
(100b)	-936.2	-1056.5	11
Average	-582.4	-667.3	

In addition, the modelling (Figure 6) results suggested an impact on the (100) and (010) faces and the morphology did change in ways that could be interpreted as these faces being expressed[31, 65].

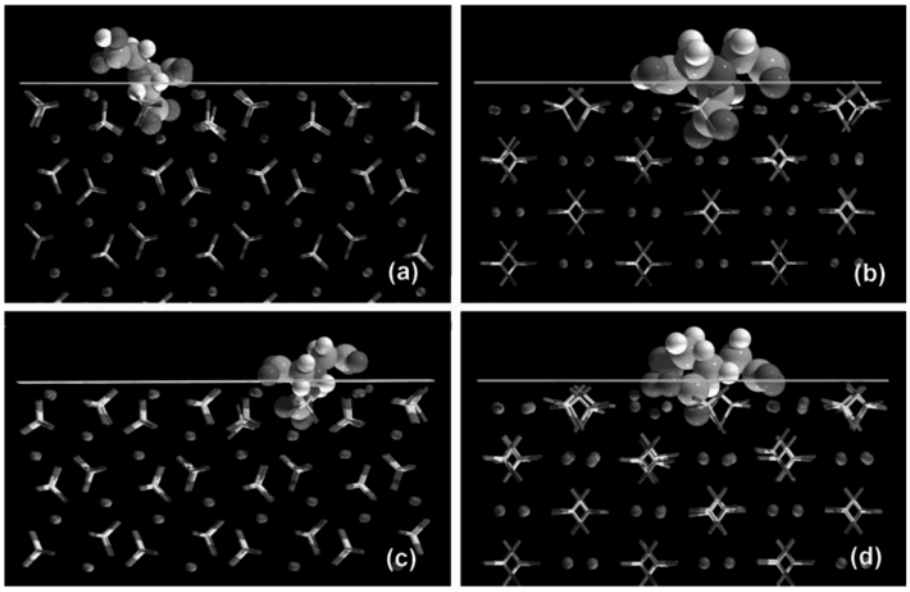

Figure 6. Molecular modelling images for the minimised energy configurations for the two lowest replacement energies of NTA adsorbed onto barium sulfate with and without the zwitterion present. (a) (100b) face - no zwitterion (b) (010) face - no zwitterion (c) (100b) face - with zwitterion (d) (010) face - with zwitterion. Adapted from Ref. 65 with permission from The Royal Society of Chemistry.

Macrocycle versus linear[78]

The impact of the organic backbone structure was investigated through the comparison of two tetra-phosphonates; one being a macrocylic structure (DOTP) while the other more linear (EDTP, see Figure 7). Comparison of the experimental data with simulation of the speciation of the organics showed that, as per the impact with the number of phosphonates, the speciation of those phosphonates is important. Thus, a critical determinant is how many of the phosphonate groups are deprotonated. Recall earlier, when discussing the MNDP molecule the modelling predicted a relatively low replacement energy but little impact on inhibition was observed experimentally. This can be understood by realising that at the

experimental pH, the charge carried by the MNDP molecule is equivalent to only one fully de-protonated phosphonate group. The model assumes all phosphonate groups are fully de-protonated. However, modelling can ask whether there are further underlying differences in the adsorption of these species even if the number of de-protonated phosphonate groups are equivalent.

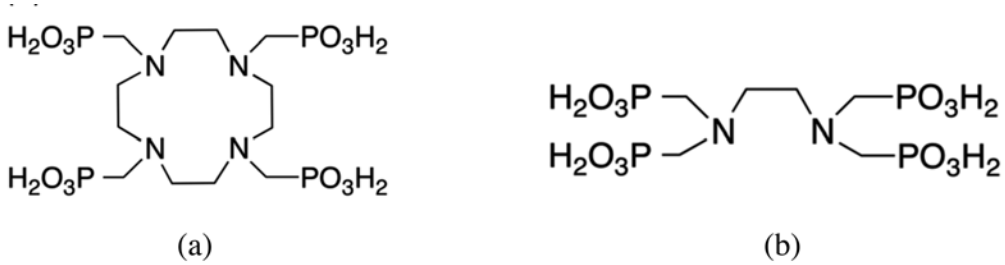

Figure 7. Linear versus macrocyclic molecules modelled (a) DOTP = 1,4,7,10-tetraazacyclododecanetetrakismethylenephosphonic acid (b) EDTP. Reproduced from Ref. 78 with permission from The Royal Society of Chemistry.

Using modelling it is seen that the macrocycle would be expected to be a weaker inhibitor (the average replacement energy is less) than EDTP according to the data in Table 5 but that both have a strong expected interaction to the (100) face of barium sulfate. In fact, the linear molecule (EDTP) has strong interactions with many barium sulfate faces while the macrocyclic (DOTP) molecule appears to have more specific interactions, with the (100) interaction much more negative than the others.

As can be seen from the data in Table 6 and ref [78], the conductivity results show that DOTP has an inhibitory impact similar to that of NTMP but that DOTP is a better inhibitor at higher concentrations. Using the average replacement energies, modelling predicts that DOTP as an inhibitor should be less potent than EDTP but more potent than NTA and just slightly more potent than NTMP. This is indeed the case according to the conductivity results.

Complexation[78]

More recently, we have used modelling to probe a scenario that is experimentally difficult to separate. That is, we have used modelling to understand whether inhibition is affected by complexation and what the drivers for this impact are. In this work we investigated the impact of DOTP in its uncomplexed or complexed with a calcium cation state. Due to the nature of the modelling this was performed by adding a calcium ion in a chelating position to DOTP and then a sulfate anion above the DOTP (away from the surface of the barium sulfate). This maintained electro-neutrality as required by this form of modelling.

The experimental results showed that complexation resulted in some loss of inhibition but not completely. That is, the complexed DOTP still showed some inhibition but that it became a weaker inhibitor as DOTP concentration increased. According to the average replacement energy (see Table 5) it predicted that this complexed molecule would be the least potent of the inhibitors tested so far. This is also borne out in the experimental results (Table 6) particularly as concentration increases. Most importantly, if only the lattice matching criteria was used, the complexed DOTP would be expected to be as strong an inhibitor as the uncomplexed molecule. Thus, the replacement energy is a better predictor than a structural comparison. As per the other molecules, the modelling was also able to correlate to the changes in morphology with the barium sulfate particles expressing flat (100) faces in the presence of DOTP (complexed or otherwise).

Table 5. Replacement energies (kJ mol^{-1}) for the free and complexed macrocyclic phosphonate on different barium sulfate faces

Face	DOTP	Complexed DOTP
(001)	-1384	-155.7
(210)	-1284	-115.3
(211)	-1558	-367.0
(010)	-1375	-585.7
(011)	-1686	-615.1
(101)	-1573	-427.5
(100a)	-2246	-957.3
(100b)	-1706	-355.7
Average	-1643.4	-447.4

Table 6. Normalised de-supersaturation rates of barium sulfate crystallised with the various organics

Concentration (mM)	EDTP	NTMP	MNDP	EDTA	NTA	DOTP	Complexed DOTP
0	1	1	1	1	1	1	1
0.0001	0.54						
0.0005	0.038		0.99				
0.0012	0.006		1.07				
0.005						0.65	0.38
0.007		0.64					
0.017±0.001		0.50		0.83		0.53	
0.026			0.88		1.15		
0.034±0.001		0.59		0.68			
0.046							0.54
0.05±0.002			1.05	0.73	0.70		
0.078					0.40		
0.091						0.31	0.70

Inorganic species[59]

Finally, while many inhibitors are indeed organic in nature, many natural waters are rich in a variety of ions, not all of which will be spectators during the process of crystallization. Here, too, modelling and the replacement energy can be used to gain insights into the possibility of incorporation and of possible ion migration[59]. This modelling showed that Ca^{2+} incorporation was more thermodynamically favourable than La^{3+} and that surface adsorption was more thermodynamically favourable over bulk incorporation. Additionally, the presence of these ions impacts on growth and morphology. Thus, there is much work to still be done in this area, especially when one considers the multitude of different ions in real, natural waters.

Conclusions

Lattice matching is a structural criteria that looks at the possibility of functional groups to sit in lattice positions. As a first approximation, this is not a bad tool. After all, the lattice positions are exactly those where the ions in the solid maximize the attractive interactions while minimizing the repulsive interactions between them. However, issues arise in using this simple criterium when comparing or trying to rank organic (or inorganic) ions as to their inhibitory potency. This is because this simple structural approach cannot take into consideration the number of functional groups, the torsional constraints within the molecules and, also importantly, the hydration energy of the respective ions. By using the replacement energy and molecular modelling, many of these factors can be taken into consideration. The replacement energy (which shows whether the adsorption reaction is favourable) has been successfully used by us to determine the relative strength of inhibition. In addition, the modelling has been relatively successful in predicting the morphological impact. This means that the replacement energy is a much better tool to predict morphological impacts and trends in inhibitory activity.

Acknowledgements

The authors would like to thank our collaborators and students who have worked with us over the years; K. Bunney, A. Baynton, T. Becker, B.D. Chandler, J. Clegg, R. de Marco, A. Fogg, S. Freeman, J.D. Gale, P. Jones, M.I. Ogden, A. Oliveira, G.M. Parkinson, S. Piana, M.M. Reyhani, W.R. Richmond, T. Radomirovic, M. Saunders, B. Skelton, G. Shimizu, A. Stanley, T. Upson.

References

1. B. Bansal and H. Müller-Steinhagen, *J. Heat Transfer*, 1993, **115**, 584-591.
2. T. R. Bott, *Fouling of heat exchangers*, Elsevier, Amsterdam, 1995.
3. *US Pat*., USXXAM US 5062962 A 19911105, 1991.
4. *European Pat*., EPXXDW EP 479465 A2 19920408, 1992.
5. D. Ester, Advanced Bleaching Technology, USA, 1997.
6. J. A. Hardy, R. T. Barthorpe, M. A. Plummer and J. S. Rhudy, *SPE Prod. Facil*., 1994, **9**, 127-131.
7. *European Pat*., EPXXDW EP 408297 A1 19910116, 1991.
8. L. F. Melo, T. R. Bott and C. A. Bernardo, *Fouling Science and Technology*, Kluwer Academic Publishers, Dordrecht, 1988.
9. *US Pat*., USXXAM US 3806451 19740423, 1974.
10. *Japan Pat*., JKXXAF JP 01104399 A2 19890421, 1989.
11. *US Pat*., USXXAM US 4937002 A 19900626, 1990.
12. *European Pat*., EPXXDW EP 297049 A1 19881228, 1988.
13. J. R. Gevecker, *Proc. Annu. Southwest. Pet. Short Course*, Lubbock, Texas, 1976.
14. E. Rizkalla, *J. Chem. Soc., Faraday Trans. 1*, 1983, **79**, 1857-1867.
15. *USSR Pat*., URXXAF SU 1231061 A1 19860515, 1986.
16. *PCT Int. Appl. Pat*., PIXXD2 WO 9106511 A1 19910516, 1991.
17. *US Pat*., USXXAM US 5116513 A 19920526, 1992.
18. L. A. Perez and D. F. Zidovc, in *Mineral Scale Formation and Inhibition*, ed. Z. Amjad, Plenum, New York, NY, USA, 1995, pp. 47-61.

19. R. Ross, K. Low and J. Shannon, *Mater. Perform.*, 1997, **36**, 53-57.
20. K. S. Sorbie and N. Laing, in *6th International Symposium on oilfied Scale*, Society of Petroleum Engineers Inc, Aberdeen Scottland, 2004, p. SPE 87470.
21. V. Tantayakom, H. S. Folger, P. Charoensirithavorn and S. Chavadej, *Cryst. Growth & Design*, 2005, **5**, 329-335.
22. M. Van der Leeden and G. Van Rosmalen, *SPE Prod. Eng.*, 1990, **5**, 70-76.
23. M. C. Van der Leeden and G. M. Van Rosmalen, *Spec. Publ. - R. Soc. Chem.*, 1988, **67 (Chem. Oil Ind.)**, 68-86.
24. *Brit. UK. Pat. Pat.*, BAXXDU GB 2328440 A1 19990224, 1999.
25. M. Yuan, M. Anderson and E. Jamieson, International Symopsium on Oilfield Chemistry, USA, 1997.
26. *UK Pat.*, EPXXDW EP 780406 A2 19970625, 1997.
27. *US Pat.*, USXXAM US 5256253 A 19931026, 1993.
28. B. C. Barja, M. I. Tejedor-Tejedor and M. A. Anderson, *Langmuir*, 1999, **15**, 2316-2321.
29. F. Jones, A. Stanley, A. Oliviera, A. L. Rohl, M. M. Reyhani, G. M. Parkinson and M. I. Ogden, *J. Cryst. Growth*, 2003, **249**, 584-593.
30. O. Nilsson and J. Sternbeck, *Geochim. et Cosmochim. Acta*, 1999, **63**, 215-223.
31. F. Jones, J. Clegg, A. Oliviera, A. L. Rohl, M. I. Ogden, G. M. Parkinson, A. M. Fogg and M. M. Reyhani, *CrystEngComm*, 2001, **40**, 1-3.
32. F. Jones, M. I. Ogden, A. Oliviera, G. M. Parkinson and W. R. Richmond, *CrystEngComm*, 2003, **5**, 159-163.
33. N. Allan, A. Rohl, D. Gay, C. Catlow, R. Davey and W. Mackrodt, *Farday Discussions*, 1993, **95**, 273-280.
34. K. Dunn, E. Daniel, P. Shuler, H. Chen, Y. Tang and T. Yen, *Journal of Colloid & Interface Science*, 1999, **214**, 427-437.
35. F. Jones, W. R. Richmond and A. L. Rohl, *J. Phys. Chem. B.*, 2006, **110**, 7414-7424.
36. A. L. Rohl, D. H. Gay, R. J. Davey and C. R. A. Catlow, *J. Am. Chem Soc.*, 1996, **118**, 642-648.
37. A. G. Stack, *J. Phys. Chem. C*, 2009, **113**, 2104-2110.
38. F. Jones, S. Piana and J. D. Gale, *Crystal Growth & Design*, 2008, **8**, 817-822.
39. S. Piana, F. Jones and J. D. Gale, *J. Am. Chem. Soc.*, 2006, **128**, 13668-13674.
40. S. Piana, F. Jones and J. D. Gale, *CrystEngComm*, 2007, **9**, 1187 – 1191.
41. U. Becker, P. Risthaus, D. Bosbach and A. Putnis, *Mol. Simulat.,* 2002, **28**, 607-632.
42. C. M. Pina, U. Becker, P. Risthaus, D. Bosbach and A. Putnis, *Nature*, 1998, **395**, 483-486.
43. Y. H. Jang, X. Y. Chang, M. Blanco, S.,Hwang, Y. Tang, P. Shuler, W. A. Goddard III, *J. Phys. Chem. B.*, 2002, **106**, 9951-9966.
44. N. de Leeuw, S. Parker and J. Harding, *Phys. Rev. B - Condensed Matter*, 1999, **60**, 13792-13799.
45. N. H. de Leeuw, *J. Phys. Chem. B.*, 2002, **106**, 5241-5249.
46. N. H. de Leeuw, *Am. Mineral.*, 2002, **87**, 679-689.
47. N. H. de Leeuw and T. G. Cooper, *Cryst. Growth & Design*, 2004, **4**, 123-133.
48. N. H. de Leeuw and S. C. Parker, *J. Chem. Soc. Faraday Trans.*, 1997, **93**, 467-475.
49. N. H. de Leeuw and S. C. Parker, *J. Phys. Chem. B*, 1998, **102**, 2914-2922.
50. J. O. Titiloye, N. H. de Leeuw and S. C. Parker, *Geochem. et Cosmochem. Acta*, 1998, **62**, 2637-2641.

51. I. Weissbuch, M. Lahav and L. Leiserowitz, *Cryst. Growth & Design*, 2003, **3**, 125-150.
52. I. Weissbuch, L. Leiserowitz and M. Lahav, in *Crystallization technology handbook*, ed. A. Mersmann, Marcel Dekker, Inc., New York, 1995, pp. 401-457.
53. S. N. Black, L. A. Bromley, D. Cottler, R. J. Davey, B. Dobbs and J. E. Rout, *J. Chem. Soc. Faraday Trans*, 1991, **87**, 3409-3414.
54. L. A. Bromley, D. Cottier, R. J. Davey, B. Dobbs, S. Smith and B. R. Heywood, *Langmuir*, 1993, **9**, 3594-3599.
55. P. V. Coveney, R. J. Davey, J. L. W. Griffin and A. Whiting, *Chem. Comm.*, 1998, 1467-1468.
56. R. Davey, S. Black, L. Bromley, D. Cottier, B. Dobbs and J. Rout, *Nature*, 1991, **353**, 549-550.
57. A. Baynton, T. Becker, B. D. Chandler, F. Jones, M. I. Ogden, T. Radomirovic and G. K. H. Shimizu, *CrystEngComm*, 2011, **13** 1090-1095.
58. M. Boon, S. R. Freeman, M. I. Ogden, A. Oliveira, W. R. Richmond, B. W. Skelton and F. Jones, *Faraday Discussions*, 2015, **179**, 343-357.
59. K. Bunney, S. R. Freeman, M. I. Ogden, W. R. Richmond, A. L. Rohl and F. Jones, *Cryst. Growth & Design*, 2014, **14**, 1650-1658.
60. S. R. Freeman, F. Jones, M. I. Ogden, A. Oliviera and W. R. Richmond, *Cryst. Growth & Design*, 2006, **6**, 2579-2587.
61. F. Jones, P. Jones, R. De Marco and B. Pjecic, *Applied Surface Science*, 2008, **254**, 3459-3468.
62. F. Jones, P. Jones, M. I. Ogden, W. R. Richmond, A. L. Rohl and M. Saunders, *J. Colloid & Int. Sci.*, 2007, **316**, 553-561.
63. F. Jones, A. Oliviera, G. M. Parkinson, A. L. Rohl, A. Stanley and T. Upson, *J. Cryst. Growth*, 2004, **270**, 593–603.
64. F. Jones, A. Oliviera, G. M. Parkinson, A. L. Rohl, A. Stanley and T. Upson, *J. Cryst. Growth*, 2004, **262**, 572-580.
65. F. Jones, A. Oliviera, A. L. Rohl, M. I. Ogden and G. M. Parkinson, *CrystEngComm*, 2006, **8**, 869-876.
66. F. Jones, A. Oliviera, A. L. Rohl, G. M. Parkinson, M. I. Ogden and M. M. Reyhani, *J. Cryst. Growth*, 2002, **237-239**, 424-429.
67. G. M. Parkinson, F. Jones, M. I. Ogden, A. Oliveira, M. Reyhani, W. R. Richmond and A. L. Rohl, *J Metastable and Nanocryst Mater*, 2005, **23**, 51-54.
68. S. Piana, F. Jones and J. D. Gale, *J. Am. Chem. Soc.*, 2006, **128**, 13668-13674.
69. J. D. Gale and A. L. Rohl, *Mol. Simulat.*, 2003, **29**, 291-341.
70. J. D. Gale and A. L. Rohl, *Mol. Simulat.*, 2007, **33**, 1237-1246.
71. F. Jones, W. R. Richmond and A. L. Rohl, *J. Phys. Chem. B*, 2006, **110**, 7414-7424.
72. A. Colville and K. Staudhammer, *American Mineralogist*, 1967, **52**, 1877-1880.
73. F. C. Hawthorn, and R. B. Ferguson, *Can. Mineral.* **1975**, *13*, 181.
74. A. L. Rohl, *Z. Kristallogr.*, 2005, **220**, 580-584.
75. F. Jones and A. L. Rohl, *Mol. Simulat.*, 2005, **31**, 393-398.
76. E. Barouda, K. D. Demadis, S. R. Freeman, F. Jones and M. I. Ogden, *Cryst. Growth & Design*, 2007, **7**, 321-327.
77. F. Jones, M. I. Ogden, G. M. Parkinson and A. L. Rohl, *CrystEngComm*, 2005, **7**, 320-323.
78. T. Radomirovic, M. I. Ogden, A. L. Rohl and F. Jones, *CrystEngComm*, 2019, **21**, 807-815.